HURRICANE MAXIMUM POTENTIAL INTENSITY AND GLOBAL WARMING

LA INTENSIDAD POTENCIAL MÁXIMA DE LOS HURACANES Y EL CALENTAMIENTO GLOBAL

A. Pérez-Alarcón[a†], J.C. Fernández-Alvarez[a], O. Díaz-Rodríguez[b]

a) Departamento de Meteorología, Instituto Superior de Tecnologías y Ciencias Aplicadas, Universidad de La Habana, Cuba; albenisp@instec.cu[†]
b) Centro de Ciencias de la Atmósfera, Universidad Autónoma de México. México
† corresponding author

Recibido 18/2/2021; Aceptado 10/10/2021

A study of the impact of global warming on the intensity of tropical cyclones (TCs) in the North Atlantic (NATL) basin for 2050, 2075 and 2100 was developed, based on the maximum potential intensity (MPI). For this study, the Geophysical Fluid Dynamics Laboratory – Climate Model (GFDL-CM4) sea surface temperature (SST) outputs and the Hurricane Maximum Potential Intensity (HuMPI) model were used. In the analysis of the mean SST on TCs season, it was observed an increase of 3^o C relative to the mean SST of 2017. For 2050, 2075 and 2100 the peak of maximum potential intensity of TCs occurs in June, displaced relative to 2017 where it is observed in July and August. In addition, a continuous increase in the MPI was verified, reaching its extreme values at the end of this century. Thus, for 2100 the maximum potential wind speed exceeds $325\ km/h$ while the potential minimum central pressure is less than $870\ hPa$. In the Gulf of Mexico, the Caribbean Sea and the Bahamas archipelago area are observed the highest values of potential intensity throughout the TCs season. Monthly, it was observed a similar behavior in all years and lower values are observed in October and November. Likewise, the theoretical intensification rates in 24 hours observed is higher than $380\ km/h$ in 2100, while the mean MPI will be 30 % higher at the end of this Century than today. Given the economic and social impact of the TCs, it is necessary to continue studying the impact of climatic change on the intensity and frequency of TCs.

Se desarrolló un estudio del impacto del calentamiento global en la intensidad de los ciclones tropicales (CTs) en la cuenca del océano Atlántico Norte (NATL) para el 2050, 2075 y 2100, basado en su intensidad máxima potencial (IMP). Para este estudio, se utilizaron las salidas de la temperatura superficial del mar (TSM) del modelo climático Geophysical Fluid Dynamics Laboratory (GFDL-CM4), así como el modelo Hurricane Maximum Potential Intensity (HuMPI). En el análisis de la TSM media durante la temporada ciclónica en NATL, se observó un incremento de 3^o C con respecto a la TSM media de 2017. Para 2050, 2075 y 2100 el pico de intensidad máxima potencial de los CTs ocurre en junio, desplazado respecto a 2017 donde se observa en julio y agosto. Además, se verificó un aumento continuo de la IMP, alcanzando sus valores extremos a fines de este siglo. Así, para 2100 la velocidad máxima del viento potencial excede los $325\ km/h$ mientras que la presión central mínima potencial es menor de $870\ hPa$. En el Golfo de México, el Mar Caribe y la zona del archipiélago de las Bahamas se observan los valores más altos de intensidad potencial durante toda la temporada de CTs. Mensualmente se observó un comportamiento similar en todos los años y se observaron valores más bajos en octubre y noviembre. De igual forma, las tasas teóricas de intensificación en 24 horas observadas superan los $380\ km/h$ en 2100, mientras que el IMP media será un 30 % superior a finales de este siglo que en la actualidad. Dado el impacto económico y social de los CTs, es necesario continuar estudiando el impacto del cambio climático en la intensidad y frecuencia de estos sistemas.

PACS: Global warming, (calentamiento global), 92.30.Np, 92.70.Mn; weather analysis and prediction (análisis y predicción del clima), 92.60.W; climate change and variability (cambio y variabilidad del clima), 92.70.Np

I. INTRODUCTION

Tropical cyclones (TCs) are one of the atmospheric events that more frequently cause natural disasters. In recent years, an increase of economic losses has been observed, which is influenced by the increase of the population in coastal areas and the increase of the economic value of infrastructures [1]. As a result, any future changes in TC activity will have significant economic and social impact, with highest impact in costal areas.

The development of new techniques aiming at improving the TC intensity and trajectory forecasting is an imperative for the international scientific community. While a continuous decrease in errors has been observed in TCs track forecast, and despite the use of sophisticated atmospheric models, there are modest advances in predicting the intensity of these systems [2, 3]. This is directly related to the uncertainties in the knowledge of the physical and dynamic mechanisms that govern the intensification and weakening of TCs. Intensity change of TCs is a complex and interactive nonlinear process that often involves several factors such as the influence of the underlying surface (e.g. the ocean) [4–6]; the internal dynamics of TCs (e.g., the inner-core structure and eyewall replacement [7–9]; and the effect of the large-scale environment (e.g., vertical wind shear and humidity) [10].

The impact of ocean conditions on the formation and maintenance of TCs is known. For example, the Sea Surface Temperature (SST) affects the latent heat, sensible heat and water vapor fluxes transported from the ocean into TCs [11, 12]. It is widely accepted that the ocean provides the energy necessary to establish and maintain secondary circulation, however, there is still no precise knowledge of how the

thermal variations of the upper layers of the ocean affect the intensity changes of TCs [6,13–15].

It has been widely accepted that TCs can be considered as a Carnot heat engine, which extracts energy from the ocean surface in the form of entropy flow, a process determined primarily by the SST [16–18], which plays an important role in the formation and intensification of these systems [19]. This is the well-known theory of Maximum Potential Intensity (MPI) developed by [18], which establishes the sea surface as a source of potential energy and, this potential energy is converted by the TC in the kinetic energy necessary to balance the friction dissipation in the mature state of the hurricane.

The SST in the regions of TC formation has increased several tenths of a degree in recent decades due to climate change [1], which combined with normal multidecadal oscillations establish ideal conditions for the formation and development of hurricanes. Furthermore, researchers from around the world have directed their efforts to understand the effect that climate change has on the TCs genesis and intensification [20]. Numerous studies have shown that TCs will be more intense and will cause more damage in the coming decades [21–23]. Emanuel [24] used an analytic model to determine an approximate expression (equation 1) for the intensification rate of a TC under favorable conditions to develop.

$$\frac{\partial V}{\partial t} = \frac{C_k}{2h}(V_{mpi}^2 - V_{max}^2) \tag{1}$$

Here V_{max} is the maximum wind speed of the TC, V_{mpi} is the TC maximum potential intensity, C_k is the nondimensional surface exchange coefficient for enthalpy and h is the boundary layer depth. It was used $h = 2$ km and $C_k = 10^{-3}$ following [25].

There is currently a strong consensus that SST will increase as a consequence of climate change. Emanuel [25], using expression 1, showed that it will be observed a rising in the intensity rates of the TC in 24 hours with the increasing of the SST, because the intensity rates depend of the square of the MPI wich is expected to increase with the SST. This behavior will make more difficult the intensity forecast of the TCs in the future.

This contribution aims to determine the maximum potential intensity that TCs could reach in years 2050, 2075 and 2100. For this, the SST outputs of the GFDL-CM4 climate model (Geophysical Fluid Dynamics Laboratory - Climatic Model version 4.0) [26] and the HuMPI (Hurricane Maximum Potential Intensity) model [27,28] will be used.

II. MATERIALS AND METHODS

II.1. GFDL-CM4

GFDL-CM4.0 is the latest version of global climate models developed by the Geophysical Fluid Dynamics Laboratory (GFDL), with the aim of making future projections of Earth clime and also to participate in the Climate Models Intercomparison Project Phase 6 (CMIP6) [29]. The objective of CMIP is to better understand past, present and future climate changes that arise from natural forced variability or in response to changes in radiative forcing in a multimodel context. Their results form the basis of a series of reports produced by the Intergovernmental Panel on Climate Change (IPCC).

GFDL-CM4.0 includes the following components: aerosol, where the GFDL-AM4 (GFDL Global Atmosphere) with a nominal horizontal resolution of 1 degree and 33 vertical levels with the top at 1 hPa was used, while for land it was used the GFDL-LM4 (GFDL Land Model) with a nominal horizontal resolution of 1 degree, 20 levels and the level below 10m. It includes dynamic vegetation and land use. On the other hand, water and ice on the ground, multilayer snow, rivers and lakes were taken into account. For the ocean, the GFDL-OM4p25 (GFDL Global Ocean and Sea Ice Model) with 0.25 degrees of resolution and 75 levels was used. For further information consult [30] and [26]. It was update for RCP8.5 (Representative Concentration Pathway). For further information about RCP8.5 see [31]. Precisely, in this study the extreme scenario RCP8.5 was used.

II.2. HuMPI

The HuMPI model was developed in the Department of Meteorology of the Higher Institute of Technologies and Applied Sciences (InSTEC), Havana University. It is composed of a modified version of MPI-theory [18] and the theory of boundary layer of the tropical cyclones described by Smith [32]. It considers the TCs as a generalized Carnot heat engine. The model works under the assumption that the TC is in a stationary state and that its intensification and persistence depend entirely on the thermal instability that exists between the ocean and the tropopause. So, the TC is powered by the latent heat transferred by evaporation from the ocean to the atmosphere through surface winds.

The model initialization requires the SST and the minimum central pressure when the system reaches the category of tropical storm. Authors in references [27, 28, 33] provide a complete description of the physical aspects and the fundamental characteristics of this model. In the simulations carried out in this research, a minimum central pressure of 1005 hPa was assumed.

II.3. Data and Methodology

The study was made for the North Atlantic basin (NATL) between 0 to 42 degrees of latitude and 250 to 358 degrees of longitude, as shown in figure 1, because the TCs are formed and develop large part of their trajectory in this area. The SST of TC season in NATL was taken from the outputs of the GFDL-CM4 for years 2050, 2075 and 2100 [30] with $0{,}25^o$ (about 25 km) of resolution, available at https://esgf-data.dkrz.de/search/cmip6-dkrz.

In addition, the MPI for Hurricane Irma (2017), Hurricane Dorian (2019) and Hurricane Lorenzo (2019) was calculated

using HuMPI model initializated with the SST outputs of the GFDL-CM4 and the high-resolution SST analysis products from infrared satellite data of the Advanced Very High Resolution Radiometer (AVHRR), available at https://www.ncei.noaa.gov/thredds/blended-global/oisst-catalog.html. The HuMPI outputs for these hurricanes will be taken as baseline.

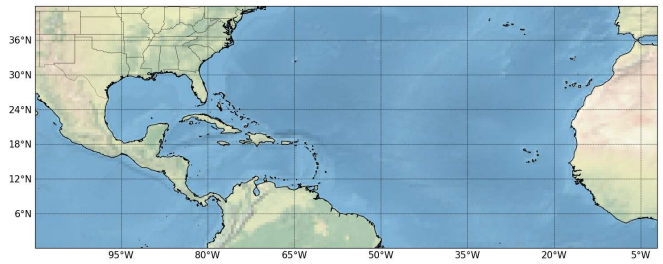

Figure 1. Study area

III. RESULTS

III.1. Hurricane Irma simulation

Hurricane Irma developed from a tropical wave originated in the west coast of Africa around August 30, 2017. The system, then a tropical depression, moved in a west-southwest direction, entering into an environment of low vertical wind shear, a low troposphere with high moisture content and a slightly warm sea surface temperature about 27^o-28^o C (figure 2). These conditions were favorable for a rapid intensification rates from tropical depression to hurricane in just 30 hours [34].

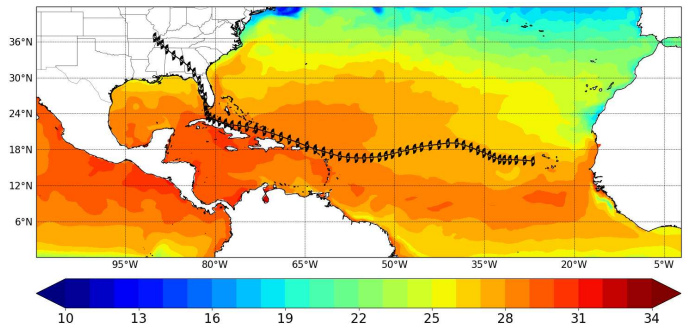

Figure 2. SST (Celsius degrees) from GFDL-CM4 for September 2017.

At the beginning of September 4, 2017, the system's eye grew in size with better definition and deep convection around the eye gained symmetry. Hurricane Irma was again in an intensification proccess, probably due to the end of a replacement cycle of the eyewall. Due to the breakdown of the western side of the mid-level anticyclonic ridge, the hurricane turned west-northwestward through another process of rapid intensification, reaching its maximum intensity of 914 *hPa* of minimum central pressure and 286 *km/h* of maximum wind speed [34].

The HuMPI model, using the SST derived from satellite products, calculated a maximum potential intensity of 310 *km/h* for maximum wind speed (figure 3a) and 902 *hPa* for minimum central pressure (figure 3b) and the theoretical intensification rates in 24 hours (equation 1) is higher than 220 *km/h*, however the maximum intensification rates observed in the system was about 85 *km/h*. From GFDL-CM4 SST outputs the calculated potential maximum wind speed is 325 *km/h* (figure 3a) and the potential minimum central pressure is 896 *hPa* (figure 3b). The simulated intensification rates is higher than 240 *km/h* in the same time lapse.

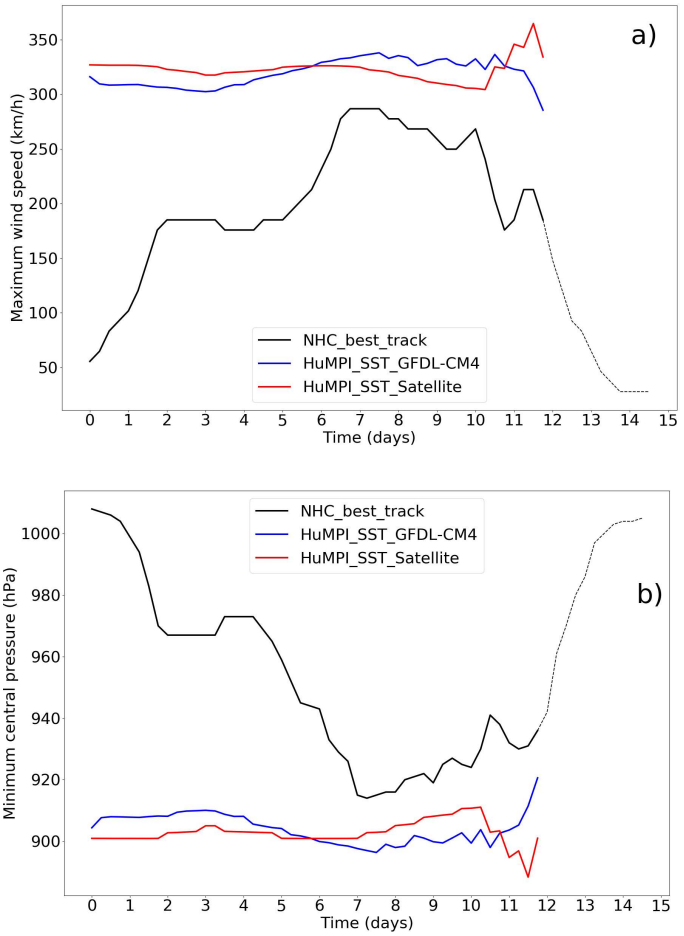

Figure 3. HuMPI simulation for Hurricane Irma (2017). (a) Potential maximum wind speed. (b) Potential minimum central pressure. Dotted lines represent the movement of the TC over land or very close to the coast. It was plotted Hurricane Irma track.

III.2. Hurricane Dorian simulation

Hurricane Dorian was formed from a tropical wave that moved westward. During its trajectory, the system moved over warm ocean waters with temperatures ranging between 27^o and 29^o C (figure 4), which made possible the rapid intensification processes that it developed during its life cycle.

Figure 5a shows that the maximum potential wind speed calculated with the HuMPI model from the SST obtained as satellite products is 313 *km/h*, while the value calculated from the SST obtained from the GFDL-CM4 is 302 *km/h*.

On the other hand, figure 5b shows that the calculated potential minimum central pressure is 904 *hPa* and 915 *hPa*, respectively. The above values are very similar to the intensity reached by Hurricane Dorian, 296 *km/h* of maximum wind speed and 910 *hPa* of minimum central pressure. Also the intensification rates experimented by Dorian were about 65 *km/h* in 24 hours while the simulated intensification rates is higher than 210 *km/h* in the same time lapse.

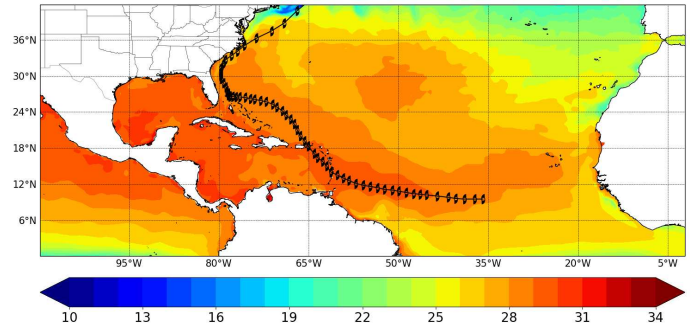

Figure 4. SST (Celsius degrees) from GFDL-CM4 for August 2019.

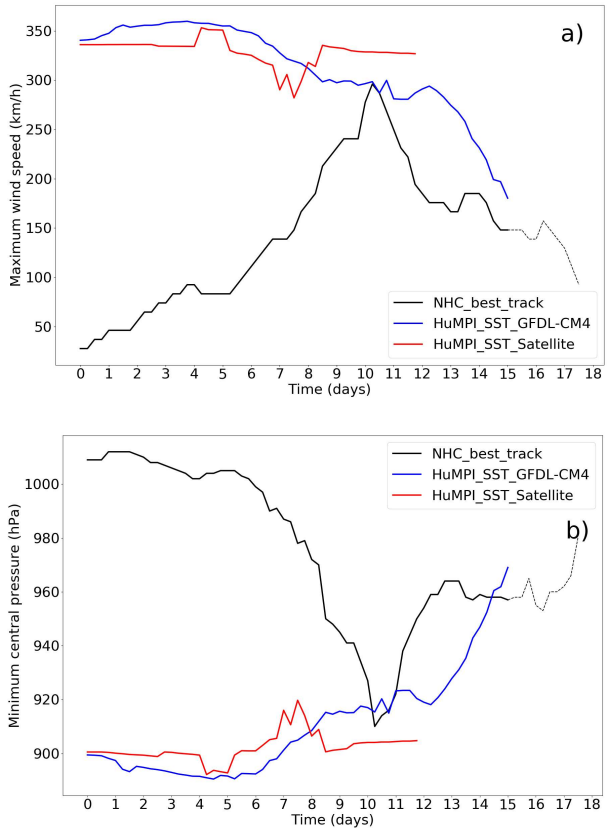

Figure 5. HuMPI simulation for Hurricane Dorian (2019). (a) Potential maximum wind speed. (b) Potential minimum central pressure. Dotted lines represent the movement of the TC over land or very close to the coast. It was plotted Hurricane Dorian track.

III.3. Hurricane Lorenzo simulation

Hurricane Lorenzo was formed from a tropical wave moving over the African coast around September, 22. Lorenzo initially moved between west and west-northwest due to the influence of a subtropical ridge to the north. By September 25, the system increased its maximum winds from 130 *km/h* to 230 *km/h* in 48 hours.

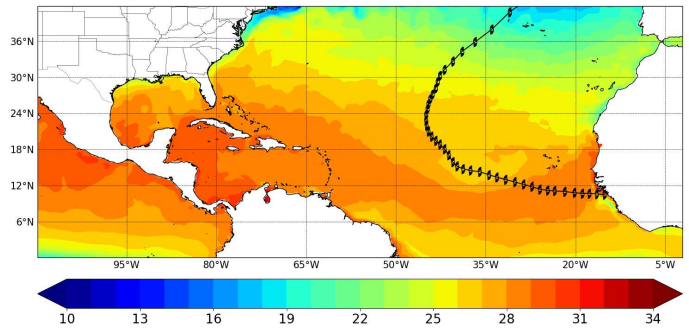

Figure 6. Mean SST (Celsius degrees) from GFDL-CM4 for September 2019.

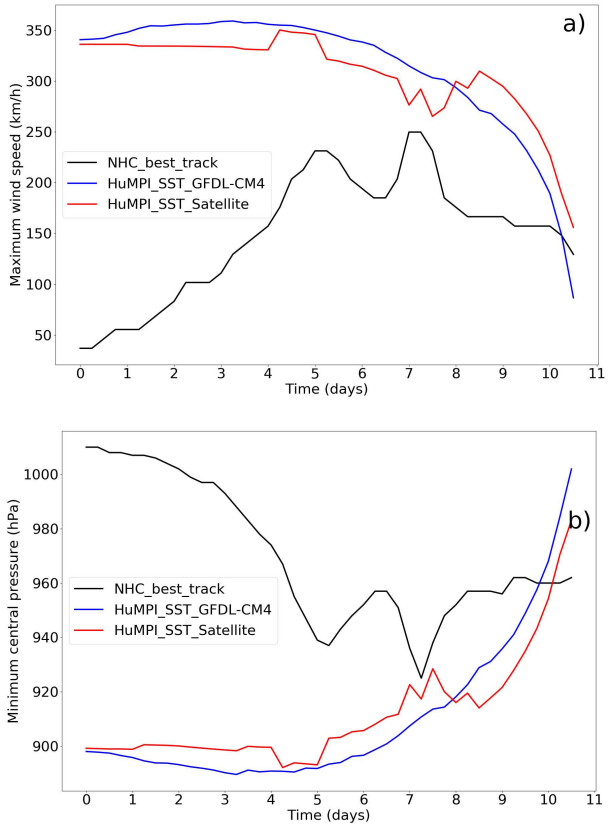

Figure 7. HuMPI simulation for Hurricane Lorenzo (2019). (a) SST Potential maximum wind speed. (b) Potential minimum central pressure. It was plotted Hurricane Lorenzo track.

The rupture of the subtropical ridge and the entry of dry air into inner core combined with a replacement cycle of the eyewall, caused Lorenzo to weaken slightly. For September 28 at 0600 UTC, Hurricane Lorenzo underwent another rapid intensification cycle by increasing the maximum wind speed by 75 *km/h* in just 21 hours, allowing it to reach its maximum intensity of 260 *km/h* and 925 *hPa* [35]. During this period the system was moving over warm ocean waters with a temperature that ranged between 26^o -27^o C (figure 6).

By September 29 at 1800 UTC, wind shear associated with an upper-level trough over the north-central Atlantic, and the

influx of drier mid-latitude air caused the system eyewall to collapse. This process and the ocean cooling from extensive upwelling associated with hurricane circulation, contributed to the weakening of Lorenzo's convective structure [35].

The HuMPI model, using SST from satellite products, simulated for Lorenzo the potential maximum wind speed is 290 km/h (figure 7a) and the potential minimum central pressure is 917 hPa (figure 7b), while for SST from GFDL-CM4 the potential maximum wind speed is 306 km/h (figure 7a) and the potential minimum central pressure is about 905 hPa (figure 7b). The intensity rates in 24 hours for Lorenzo applying equation (1) is greater than 200 km/h in 24 hours.

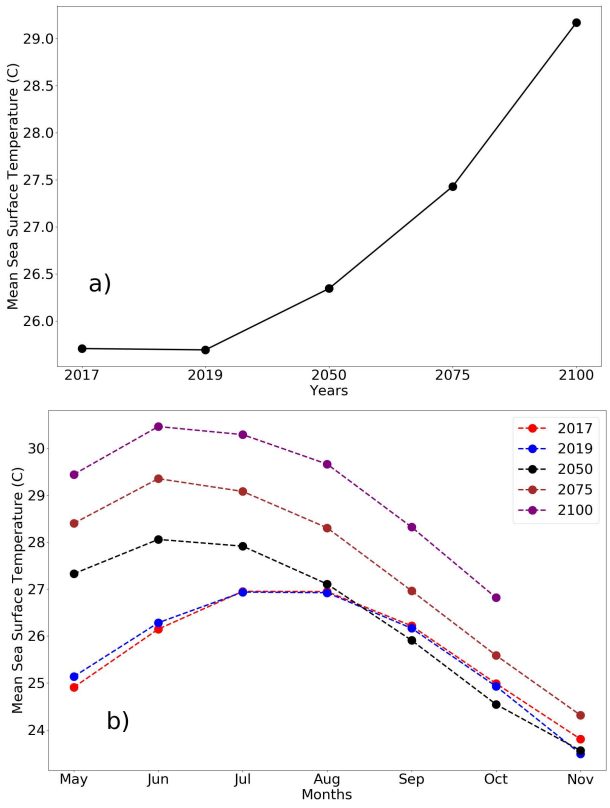

Figure 8. Mean SST (Celsius degrees) evolution from GFDL-CM4 . (**a**) annual (from May to November) (**b**) monthly

In summary, the results shown in Figures 3, 5 and 7 corroborate the ability of the HuMPI model to calculate the maximum potential intensity of hurricanes in NATL. Furthermore, it is easy to verify how the potential intensities calculated using the SST from GFDL-CM4 and the SST derived from satellite products show a similar behavior during the life cycle of the analyzed TCs. This result allows to use the GFDL-CM4 SST output to calculate de hurricane maximum potential intensity for 2050, 2075 and 2100.

III.4. SST evolution

Figure 8a shows the evolution of the mean SST from May to November in NATL over the area between the equator and 42^o of latitude. This is the zone where TCs are formed and intensified in NATL basin. It is remarkable how for 2100 occurs an increase in the mean SST of about 3^o C respect to 2017. In fact, it is observed a continuous increase in the SST from 2017 to 2100. These results are in agreement with [36]. For a complete review of the GFDL-CM4 performance consult [36] and [29].

Figure 8b shows the mean SST from May to November. The maximum mean SST values are observed in July and August for 2017 and 2019, however, for 2050, 2075 and 2100 the maximum value is displaced to June and July, reaching values above 30^o C for June 2100. This increase in SST has a proportional impact on the TC potential intensity.

This behavior demonstrates the significant impact that global warming has on ocean temperatures. For TC genesis, the SST must be higher than 26^o Celsius [37–39]. The previous results show that in the coming decades this temperature threshold will be exceeded in larger ocean areas with greater depths. So, it will increase considerably the favorable oceanic conditions for TCs formation.

III.5. Hurricane potential intensity for 2050, 2075 and 2100

Figure 9 shows the potential intensity calculated for TCs in 2050. In general, it is easy to observe wind speeds larger than 300 km/h and the minimum central pressure below 890 hPa for June and July, in the area untill 30^o of latitude.

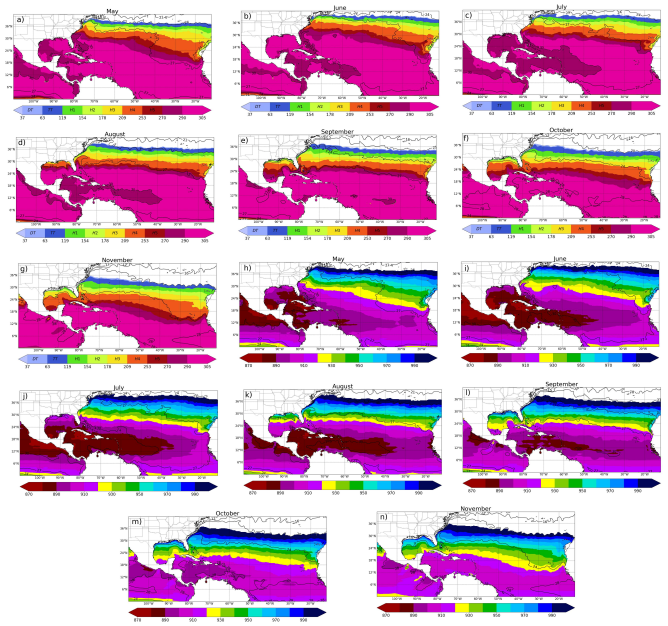

Figure 9. HuMPI outputs from May to November of 2050 with SST taken from GFDL-CM4. (a-g) Potential maximum wind speed (km/h). (h-n) Potential minimum central pressure (hPa).

TCs rarely occur outside the hurricane season (between June and November) [40], however, according to Fig. 9, it is remarkable to see the large values of MPI obtained for the month of May which may indicate an earlier start for future hurricane seasons. For October and November the extreme values are located in the Gulf of Mexico, the Caribbean Sea and the region between the Arc of the Lesser Antilles and the African coast. Nevertheless, intensities higher than those

of a category 3 hurricane on the Saffir-Simpson scale, can be reached at about 30^o latitude.

For year 2075, figure 10 shows more regions with intensities higher than 312 km/h for wind speed and less than 880 hPa for minimum central pressure in June, July and August. For November the highest intensities are observed below 25^o of latitude. This increasing of the maximum potential intensity of the TCs compared to 2050 is in correspondence with the rising of SST shown in figure 8.

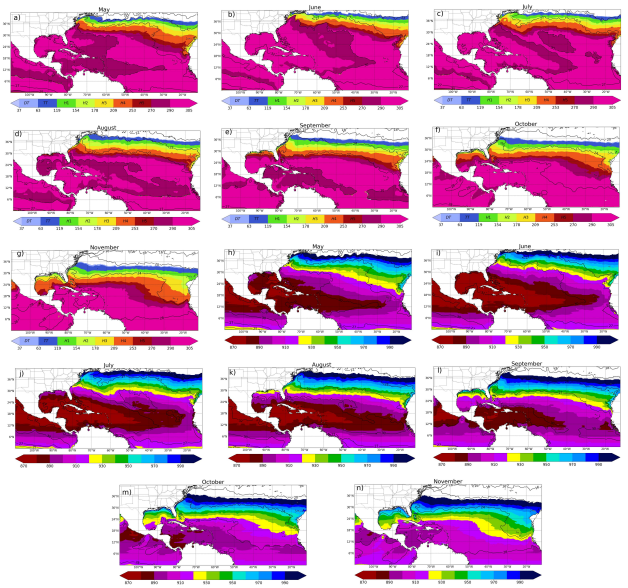

Figure 10. HuMPI outputs from May to November of 2075 with SST taken from GFDL-CM4. (a-g) Potential aximum wind speed (km/h). (h-n) Potential minimum central pressure (hPa).

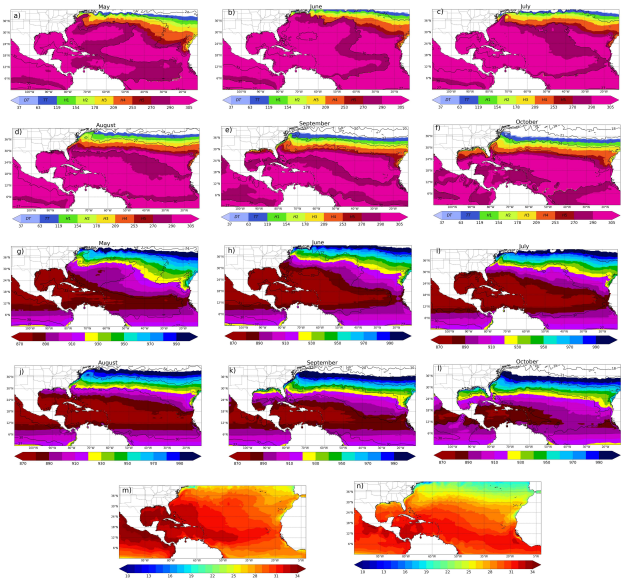

Figure 11. HuMPI outputs from May to October of 2100 with SST taken from GFDL-CM4. (a-f) Potential maximum wind speed (km/h). (g-l) Potential minimum central pressure (hPa). (**m-n**) SST (Celsius degree) for July and September of 2100.

The TC potential intensity calculated for 2100 has wind speeds larger than than 325 km/h and a minimum central pressure lower than 870 hPa. For June, July and August it is observed that the extreme values in the maximum wind speed cover more than 90 % of the study area, while in the Caribbean Sea, Gulf of Mexico as well as the zone between 10^o and 20^o of latitude are observed the lowest values of the potential minimum central pressure (figure 11).

Figure 11m and Figure 11n show the SST for July and September. The SST in the Caribbean Sea, Gulf of Mexico and the coast of the Bahamas archipelago will be larger than 32^o C on July. Also, SST values higher than 34^o C are observed in some areas of them. For September a decreasing in the SST is observed, although SST is higher than 30^o C.

Table 1 shows the TC theoretical intensification rates in 24 hours assuming that the TC development is not disturbed by detrimental environmental conditions such as vertical wind shear. It is remarkable the increasing of this rates, varying from 230 km/h in 2017 to values higher than 380 km/h in 2100.

Table 1. TC theoretical intensification rates in 24 hours applying equation (1). For this analysis, it was assumed a TC with a maximum wind speed of 185 km/h.

Years	Intensification rates
2017	230 km/h
2019	230 km/h
2050	270 km/h
2075	$\sim$ 320 km/h
2100	$>$ 380 km/h

IV. DISCUSSION

Figures 8 and 12 show the proportional dependency that exists between the MPI and the SST. Figure 12a shows a continuous increase in the mean MPI of the TC in NATL, reaching values about 340 km/h in maximum wind speed in 2100, while the minimum central pressure drops to 895 hPa (Figure 12b) by the end of this century.

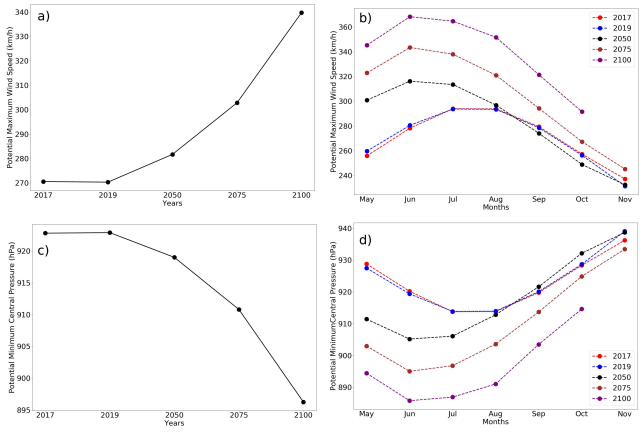

Figure 12. Mean TC maximum potential intensity. (a-b) maximum wind speed (c-d) minimum central pressure

Monthly is observed a displacement of the peaks of the mean MPI to June in 2050, 2075 and 2100 (figures 12c and 12d) as it was discuss in Section "Hurricane potential intensity for 2050, 2075 and 2100respect to mean MPI in 2017 and 2019, in correspondence with what was observed in the trend of the mean SST (figure 8b).

The results presented in this research are consistent with the climatological effects of SST on the intensity and intensity changes of tropical cyclones. In fact, Cione and Uhlhorn [6] demonstrated that the changes in the SST are directly linked to TC intensity and suggested a relationship between inner core-ocean cooling and TC intensification. Indeed, the TC intensification extracting heat energy from the ocean surface [6, 12, 18] leads to an up-welling of colder deep waters that results in a cooling of the SST under the TC inner core [41].

For 2100, in the TC official season, it is observed an increase of approximately of 3^o C in the mean SST respect to 2017, which have a direct impact on the TC intensification. That was demonstrated through the calculation of the MPI. Author in ref. [42] showed that the mean TC intensification increases by 16 % for every 1^o C increase in mean SST. Thus, based on our findings, hurricanes in 2100 will be 48 % more intense than today.

Furthermore, the theoretical intensity rates in 24 hours are directly proportional to the MPI [25], so the largest intensity changes will be observed in the Caribbean Sea and the Gulf of Mexico. In these areas generally occur the processes of rapid intensification of hurricanes in the NATL [43]. Bhatia et al. [44] detected a slight increase in the TCs intensification rates in NATL with a positive contribution from anthropogenic forcing, however, they suggest the need for thorough studies to be able to detect a solid trend on a global scale. Additionally, figures 9, 10 and 11 show that the highest MPI are located in the intra-American Seas and the Western Atlantic Ocean. Strazzo et al. [45] found that TCs have greater sensitivity to changes in SST in these areas.

However, it is unclear the mechanism of the effect of global warming on the intensity of TCs. The increasing of SST will enhance the convection over the ocean and thus the upper troposphere tends to be warm due to more latent heat loss, which causes a more stable atmospheric stratification and inhibits the formation and development of TCs. Moreover, there is a negative feedback between the TCs and ocean: when TCs pass through the ocean, cold thermocline water is entrained into the mixed layer and SST decreases, leading to the decreasing of latent heat flux from ocean to atmosphere and weakens the intensity of TCs.

Additionally, future projections of TC activity are subjected to uncertainties in climate projections such as climate-forcing scenario and model dynamics and physics. According to Roberts et al. [46], the spatial resolution (~ 100km) of climate models generally cannot simulate category 4-5 hurricanes, but higher-resolution global models (~10–100-km of horizontal resolution) reproduce a more realistic TC structure. Despite these limitations, the findings of several authors [47–51] suggest an increase in the TC intensity with global warming, as we found here. Conversely, other studies [52–55] have addressed that the frequency of TCs increases with global warming, but not TC intensity.

In summary, the increase in the TCs intensity due to global warming will cause that TCs will have a better define convective structure and therefore an increase in rainfall associated to them. This phenomena, together with the rising of the sea level due to the melting-ice, would cause serious damage to the Caribbean Islands and to the all coastal population affected annually by TCs. As a consequence, an increase in economic damage would occur due to the displacement of people and their goods to safe places, as well as the damage to the infrastructures located in the coastal zone.

V. CONCLUSIONS

An attempt is made to understand the consequences of increase of SST due to climatic change in TC intensity and intensification rates by performing numerical simulations with HuMPI model. Like [18, 56, 57], the HuMPI model predicts an increase of the maximum potential intensity with increasing SST. Indeed, the impact of the SST on the maximum potential intensity of the TCs was again verified.

Thus, future TCs will have higher wind speeds. By the end of the 21st Century, the peak of the MPI will be observed in June, while the Caribbean Sea and Intra-American Seas could be the areas where the TCs would reach the maximum potential intensity. In addition, a significant increase in intensification rates in 24 hours will be expected for 2100 and the mean MPI will be 30 % higher at the end of this century than today.

Finally, given the impact that tropical cyclones have on the social and economic life of people, it is necessary to continue to develop research to determine the impact of global warming on both the intensity and frequency of tropical cyclones, especially those that reach higher intensity than a category 3 hurricane on the Saffir-Simpson scale.

ACKNOWLEDGEMENTS

The authors acknowledge the availability of public datasets from the GFDL-CM4 model and the U. S National Climatic Data Center. The authors also owe thanks to Alfo José Batista-Leyva from the Department of Atomic and Molecular Physics, Higher Institute of Technology and Applied Sciences, University of Havana and Rogert Sorí-Gómez from the Environmental Physics Laboratory, Faculty of Science, University of Vigo, for their recommendations and suggestions.

REFERENCES

[1] T. Knutson, J. Mcbride, J. Chan, K. Emanuel, G. Holland, C. Landsea, I. Held, J. Kossin, K. Srivastava, M. Sugi, Nat. Geosci. **3**, 157 (2010).
[2] E. N. Rappaport, J.-G. Jiing, C. W. Landsea, S. T. Murillo, J. L. Franklin, Bull. Am. Meteorol. Soc. **93**, 371 (2012).
[3] K. Balaguru, G. R. Foltz, L. R. Leung, S. M. Hagos, D. R. Judi, Weather Forecasting **33**, 411 (2018).
[4] L. F. Bosart, W. E. Bracken, J. Molinari, C. S. Velden, P. G. Black, Mon. Weather Rev. **128**, 322 (2000).
[5] L. K. Shay, G. J. Goni, P. G. Black, Mon. Weather Rev. **128**, 1366 (2000).

[6] J. J. Cione and E. W. Uhlhorn, Mon. Weather. Rev. **131**, 1783 (2003).
[7] J. Kaplan and M. DeMaria, Climatological and synoptic characteristics of rapidly intensifying tropical cyclones in the North Atlantic basin. Preprints 23rd Conf. on Hurricanes and tropical Meteorology, Dallas, TX (1999).
[8] M. Sitkowski, J. P. Kossin, C. M. Rozok, Mon. Weather Rev. **139**, 3829 (2011).
[9] S. Gao, S. Zhai, L. S. Chiu, D. Xia, J. Appl. Meteorol. Climatol. **55**, 425 (2016).
[10] R. L. Elsberry, L. Chen, J. Davidson, R. Rogers, Y. Wang, L.Wu, Trop. Cyclone Res. Rev. **2**, 13 (2013).
[11] G. J. Holland, R. T. Merrill, Q. J. R. Meteorolog. Soc. **110**, 723 (1984).
[12] G. J. Holland, J. Atmosph. Scie. **54**, 2519 (1997).
[13] K. Balaguru, P. Chang, R. Saravanan, L. R. Leung, Z. Xu, M. Li, J.-S. Hsieh, Proc. Natl. Acad. Sci. U. S. A. **109**, 14343 (2012).
[14] S. A. Grodsky, N. Reul, G. Lagerloef, G. Reverdin, J. A. Carton, B. Chapron, Y. Quilfen, V. N. Kudryavtsev and H.-Y. Kao, Geophys. Res. Lett. **39**, (2012).
[15] C. Maes, T. J. O'Kane, J Geophys Res C: Oceans **119**, 1706 (2014).
[16] E. Kleinschmidt, Meterol. Atmos. Phys. **4**, 53 (1951).
[17] J. S. Malkus and H. Riehl, Tellus **12**, 1 (1960).
[18] K. A. Emanuel, J. Atmos. Sci. **43**, 585 (1986).
[19] J. Xu, Y. Wang, Weather Forecasting **33**, 523 (2018).
[20] E. D. Gutmann, R. M. Rasmussen, C. Liu, K. Ikeda, C. L. Bruyere, J. M. Done, L. Garre, P. Friis-Hansen, V. Veldore, J. Clim. **31**, 3643 (2018).
[21] M. E. Mann and K. A. Emanuel, EOS Trans. Am. Geophys. Union **87**, 233 (2006).
[22] R. Mendelsohn, K. Emanuel, S. Chonabayashi, L. Bakkensen, Nat. Clim. Change **2**, 205 (2012).
[23] K. A. Emanuel, Weather Clim. Soc. **3**, 261 (2011).
[24] K. A. Emanuel, J. Atmos. Sci. **69**, 988 (2012).
[25] K. A. Emanuel, Bull. Am. Meteorol. **98**, 495 (2017).
[26] I. M. Held, *et al*. J. Adv. Model Earth Syst. **11**, 3691 (2019).
[27] A. Perez-Alarcón, Diploma Thesis Instituto Superior de Tecnologías y Ciencias Aplicadas, Havana, July, 2015 (2015).
[28] A. Perez-Alarcón, J. C. Fernández-Alvarez and O. Díaz-Rodríguez, Rev. Cubana Fis, **38**, 85 (2021).
[29] M. Winton, *et al.*, J. Adv. Model Earth Syst. **12**, e2019MS001838 (2020).
[30] H. Guo, *et al.*, NOAA-GFDL GFDL-CM4 model output (2018).
[31] K. Hayhoe, J. Edmonds, R. E. Kopp, A. LeGrande, B. Sanderson, M. Wehner, D. Wuebbles, In: Climate Science Special Report: Fourth National Climate Assessment I, 133 (2017).
[32] R. K. Smith, Q. J. R. Meteorolog Soc. **129**, 1007 (2003).
[33] J. C. Fernández-Alvarez, O. D. Rodríguez, A. Pérez-Alarcón, Rev. Bras. Met. 34, 101 (2019).
[34] P. J. Cangialosi, A. S. Latto, R. Berg, National Hurricane Center Tropical Cyclone Report. Hurricane Irma, Technical report, National Hurricane Center (2018).
[35] D. A. Zelinsky, National Hurricane Center Tropical Cyclone Report. Hurricane Lorenzo, Technical report, National Hurricane Center (2019).
[36] C. Murphy, P. Gardoni and R. McKim, Climate Change and Its Impacts Risks and Inequalities, Climate Change Management (Springer International Publishing AG, Gewerbestrasse 11, 6330 Cham, Switzerland, 2018).
[37] W. Gray, Mon. Weather Rev. **96**, 669 (1968).
[38] W. Gray, Meteorol. Atmos. Phys. **67**, 37 (1998).
[39] R. A. Dare and J. L. McBride, J. Clim. **24**, 4570 (2011).
[40] H. Ramsay, Oxford University Press (2017).
[41] S. Jullien, P. Marchesiello, C. E. Menkes, J. Lefevre, N. C. Jourdain, G. Samson, M. Lengaigne, Clim. Dyn. **43**, 2831 (2014).
[42] E. Fraza, J. B. Elsner, Prog. Phys. Geogr. **36**, 395 (2015).
[43] P. H. Yaukey, Int. J. Climatol. **34**, 1038 (2014).
[44] K. T. Bhatia, G. A. Vecchi, T. R. Knutson, H. Murakami, J. Kossin, K. W. Dixon, C. E. Whitlock, Nat. Commun. **10**, 635 (2019).
[45] S. Strazzo, J. B. Elsner, J. C. Trepanier, K. A. Emanuel, J. Adv. Model Earth Syst. **5**, 500 (2013).
[46] M. Roberts, P. Vidale, C. Senior, H. Hewitt, C. Bates, S. Berthou, P. Chang, H. Christensen, S. Danilov, M.-E. Demory *et al.*, Bull. Am. Meteorol. Soc. **99**, 2341 (2018).
[47] K. Emanuel, R. Sundararajan and J. Williams, Bull. Am. Meteorol. Soc. **89**, 347 (2008).
[48] K. Emanuel and A. Sobel, J. Adv. Model. Earth Syst. **5**, 447 (2013).
[49] J. V. Manganello, *et al.*, J. Clim. **27**, 7622 (2014).
[50] K. Balaguru, G. R. Foltz, L. R. Leung and K. A. Emanuel, Nat. Commun. **7**, 1 (2016).
[51] T. Knutson, S. Camargo, J. Chan, E. Kerry, H. Chang-Hoi, K. James, M. Mrutyunjay, S. Masaki, S. Masato, W. Kevin *et al.*, Bull. Am. Meteorol. Soc. **10**, 303 (2019).
[52] S. J. Camargo, J. Clim. **26**, 9880 (2013).
[53] H. Murakami, P.-C. Hsu, O. Arakawa, T. Li, J. Clim. **27**, 2159 (2014).
[54] M. Wehner, *et al.*, J. Clim. **28**, 3905 (2015).
[55] K. Bhatia, G. Vecchi, H. Murakami, S. Underwood, J. Kossin, J. Clim. **31**, 8281 (2018).
[56] B. I. Miller, J. Meteorol. **15**, 184 (1958).
[57] K. A. Emanuel, J. Atmos. Sci. **45**, 1143 (1988).